Impact of particle shape on networks in sands

Wenbin Fei [a], Guillermo A. Narsilio [a,*], Joost H. van der Linden [a], Antoinette Tordesillas [b], Mahdi M. Disfani [a], J. Carlos Santamarina [c]

[a] Department of Infrastructure Engineering, The University of Melbourne, Parkville, Australia
[b] School of Mathematics and Statistics, The University of Melbourne, Parkville, Australia
[c] Energy Resources and Petroleum Engineering, King Abdullah University of Science and Technology, Thuwal 23955-6900, Saudi Arabia

ARTICLE INFO

ABSTRACT

Employing network science to understand particle interactions helps manufacture advanced materials with superior force transmission and heat transfer. However, knowledge of the dependence of networks on particle features such as shape is missing. This study computes particle shape — the average of three-dimensional sphericity and roundness, and multiscale network variables — *degree, edge betweenness centrality* and *global clustering coefficient* from unweighted/weighted contact and thermal networks — for three sands based on their X-ray computed tomography images. The dependence of network features on particle shape is explored for both individual particles and bulk sand samples. Results show that particle shape affects the degree in a network at sample and particle scales differently. In contrast, weighted edge betweenness centrality has a consistent inverse relationship with particle shape at both scales. The weighted edge betweenness centrality values from different samples consistently indicate that 20% of network edges (e.g., contacts) are responsible for 60% of the heat transfer in dry sands. Although unweighted edge betweenness centrality cannot reflect the heat transfer directly, it has a similar correlation with particle shape to the weighted feature. Global clustering coefficient from the thermal network increases in round particle packings and can indicate the mechanical rigidity of sands.

1. Introduction

Granular materials that surround us in engineering projects and daily life, such as sands, grains, snow and candy, are assemblies made of discrete particles in contact, and they can behave as solids (e.g., ground) or liquids (e.g., grains flowing out of a silo). The behaviour of a granular material, in essence, is a presentation of how interior particles interact spatially and temporally. In material science, defining the particle features such as size, shape, orientation and the particle connectivity patterns can help produce metamaterials with superior bulk properties in mechanical (Vangelatos et al., 2020), thermodynamical (Wang et al., 2017), acoustic (Lepidi and Bacigalupo, 2018) and electromagnetic (Lin et al., 2020) fields of research. It is known that the interaction between particles is mainly controlled by two aspects: the inherent particle features and external loading (Fei and Narsilio, 2020b, Quezada et al., 2014). Hence, characterising and fundamentally understanding the impact of particle features on particle interaction is crucial to design and manufacture granular materials with desired properties, particularly related to the foci of this paper: force transmission and heat transfer.

In a granular material, the interaction between particles determines its microstructure, which can be presented at diverse scales. In a local neighbourhood of a particle, the *coordination number* is used to measure the number of its contacts with its neighbours. Particles can also "push" other particles to transmit force when the granular material is subjected to a mechanical loading. Hence, natural constructs such as *force chains* (Tordesillas et al., 2015b, Gong et al., 2019, Imseeh and Alshibli, 2018) can be used to quantify the microstructure at a larger scale (longer distance). At a bulk scale, parameters such as *porosity* which measures the fraction of solid particles in a sample (a mix of solid particles and void space), may indicate the probability of particle interactions. However, "measuring" some of these multiscale microstructural features can be challenging, especially for natural sands in which particles have irregular shapes — elongated, platy, convex, concave, etc. Recently, network science tools are becoming more utilised and developed to characterise the microstructure using complex network theory (Papadopoulos et al., 2018, Newman, 2003, Fei et al., 2020, Tordesillas et al., 2015a, Walker and Tordesillas, 2010) and to study physical processes using network models (Yun and Evans, 2010, Gostick et al., 2016, Fei

---

* Corresponding author at: Engineering Block B 208, Department of Infrastructure Engineering, The University of Melbourne, Parkville, VIC 3010, Australia.
E-mail address: narsilio@unimelb.edu.au (G.A. Narsilio).

et al., 2019b).

In network science, a network is a web of nodes and edges with varying definitions to render different networks. For example, in a *contact (force)* network, a node is assigned to each particle centroid and an edge is generated at each particle contact (Nie et al., 2020). In contrast, a node represents a pore space and an edge indicates a pore throat in a *pore* network (Birkholz et al., 2019). Based on these networks, complex network theory can be used to calculate network variables or "features" including *degree*, *centrality*, *betweenness*, *cycles* and *clustering coefficient* (Papadopoulos et al., 2018). By using these new features, the relationship between microstructure and macroscale physical behaviours such as mechanical stability (Brocato, 2020), permeability (van der Linden et al., 2016) and effective thermal conductivity (Fei et al., 2019b) have been studied. This approach will facilitate the investigation of heat transfer at the microscale and mesoscale (chain) scale on top of the existing microstructural factors such as particle size (Gan et al., 2017a, Chari et al., 2013, Zhang et al., 2015), particle shape (Mirmohammadi et al., 2019, Fei et al., 2019a, Lee et al., 2017) and structure-related index (Dai et al., 2019, Siu and Lee, 2000, Kovalev and Gusarov, 2017). Nevertheless, many of these studies focus on sphere packings while research on how the features of particles affect the network architectures is still lacking. Although Papadopoulos et al. (2018) raised the open question of "which (quantitative and qualitative) aspects of network structure depend on features of grains (such as shape, polydispersity, friction, cohesiveness, and so on) and which are more universal.", few studies have been conducted on this topic.

Particle shape is one of the key particle features in material selection and it strongly influences contact response (Nadimi et al., 2019, Cho et al., 2006, Santamarina and Cho). Even though recent studies have shown the interest in the complex systems made of particles with non-sphere particles such as ellipses (Schreck et al., 2010), squares and rods (Hidalgo et al., 2009, Trepanier and Franklin, 2010), Z-shape particles (Murphy et al., 2016) and U-shaped particles (Gravish et al., 2012), representations of the systems as networks are missing and the relationships between particle shape and network features have yet to be explored in detail. Introducing a proper approach to quantify the shape of particles in natural granular materials could be challenging due to particles in soils and rocks having complex shapes and rough surfaces. Constructing unweighted networks for natural sands is challenging, since advanced techniques such as micron-resolution Computed Tomography (μCT) and image processing are required to capture the particle location and detection contacts indestructibly. It is more difficult to establish weighted networks; for example, in force networks contact force and the contact area can be used as weights, however these are hard to quantify accurately, particularly between irregularly shaped particles. Additionally, widely used contact (force) networks may be insufficient for studying heat transfer which occurs not only through the interparticle contacts but also through the (small) gaps between particles in dry materials and through any connected liquid phases in the void space in unsaturated systems. Hence, it is desirable to build new networks such as a thermal network that considers the gaps for dry granular materials, but only few studies are found in the literature.

This paper aims to investigate the dependence of network features on particle shape at multiple spatial scales. Three sands with distinct particle shapes are selected for μCT under different compressive states over time. Based on the μCT images, three-dimensional (3D) sphericity and roundness are computed to describe particle shape. For each sand under each loading stage, a contact network and a thermal network are constructed, weighted with the intention to capture the sparsely distributed force transmission and heat transfer. Three network features — degree, edge betweenness centrality, global clustering coefficient — are extracted from the networks using complex network theory, representing different length scales in the packings. The impact of particle shape on the three network features for individual particles and the particle packings is investigated.

2. Materials

Three sands are selected in this work as shown in Fig. 1: Glass beads, Ottawa sand, and Angular sand. The particles in these sands have distinct shape but similar equivalent diameter (Table 1). Glass beads are round with silver coatings as shown at the top right in Fig. 1 (a). Ottawa sand 20–30 is a standard sand (ASTM, 2017) often used in geotechnical engineering research and the particles are elongated but with smooth surfaces. Compared with particles in Ottawa sand, Angular sand is made of particles with more irregular shapes and even concave areas in the particle surface. Each sand is air-pluviated in a cylindrical container 25 mm in diameter and 25 mm in height. The samples are scanned using μCT to obtain sequential images with a pixel size of 13 *μm* in three loading stages (i.e., 0 – 2.0 – 6.1 – 10.2 MPa). The CT images of Ottawa sand and Angular sand, and their corresponding networks are accessible to researchers (Fei and Narsilio, 2021, Fei et al., 2021). From CT images of each sand, four cubic regions of interests (ROIs) with a side length of 4.5 mm are cropped from its top-left, top-right, bottom-left and bottom-right to minimise the effect of heterogeneity on the analysis in this paper. The amount of particles in each ROI of Glass beads, Ottawa sand and Angular sand is around 270, 120 and 100, respectively.

3. Particle shape descriptors

Particle shape descriptors can characterise different length scales. Here we use sphericity/elongation, roundness/angularity and roughness/smoothness as shape descriptors across the three scales (Santamarina and Cho, 2004). Sphericity is at the length scale of the particle diameter and it measures the extent that the particle approaches a sphere. Roundness is at the same length scale as the particle corners, it measures the extent that the corner can be rounded. Roughness is at the smallest scale of individual particle characterisation and focuses on the particle surface, from a pragmatical point of view, it is on the same scale as the resolution of CT images.

Selecting the CT resolution is a trade-off between obtaining images with higher resolution but on a smaller sample size and images with lower resolution but on a larger sample size. CT images with a resolution of 1*μm* is desired (Kerckhofs et al., 2012) to characterise the roughness of particle surface while larger samples are required to study the particle connectivity in this work. Hence, we selected the CT image resolution as 13 *μm* and concentrated on sphericity and roundness for characterising particle shape. This choice is supported by recommendations made in recent literature based on a comparison of different definitions (or equations) of various particle shape descriptors (Fei et al., 2019a). Although sphericity (S) can be quantified using particle radii or principle axial lengths, the resulting S may not be able to distinguish shape of all natural sands. Thus, following the recommendation and framework in (Fei et al., 2019a), Eqs. (1) and (2) were used for computing sphericity (S) and roundness (R) based on smooth individual particles extracted from the CT images.

$$S = \frac{36\pi V^2}{SA^3} \tag{1}$$

where V is the particle volume, SA is the particle surface area. The selected 13 *μm* resolution may introduce an error in SA, however using other definitions of S (e.g., particle radii) may result in a larger error in characterising particle shape, a limitation only resolved by increasing image resolution at the cost explained earlier.

$$R = \frac{\sum r_i/N}{r_{max-in}} \tag{2}$$

where N is the number of corners, r_i is the radius of the a particle corner and r_{max-in} is the radius of the maximum inscribed sphere in the particle as shown in Fig. 2 .

Glass beads   Ottawa sand   Angular sand
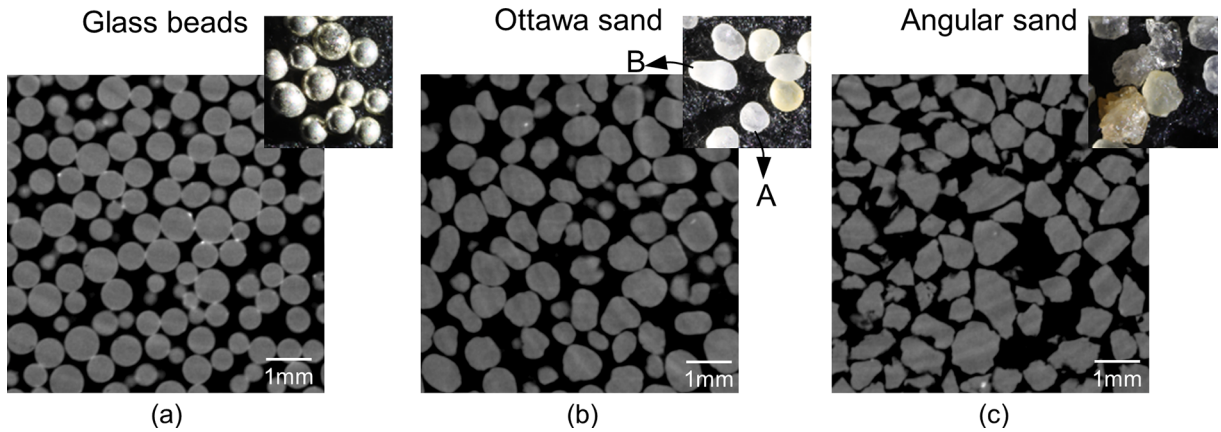
Fig. 1. The computed tomography (CT) images of three sands: (a) Glass beads, (b) Ottawa sand and (c) Angular sand.

Table 1
Particle size of the studied granular materials.

Sample	D_{50}(mm) *	D_{50}(mm) ^	Particle size range (mm) *	Particle size range (mm) ^
Glass beads	0.60	0.60	0.50 – 0.70	0.40–0.80
Ottawa sand	0.73	0.76	0.60 – 0.85	0.58–0.94
Angular sand	0.89	0.68	0.60 – 1.18	0.39 – 0.99

* Diameter from sieve analysis.
^ Equivalent ball diameter derived from particle volume after CT reconstruction.
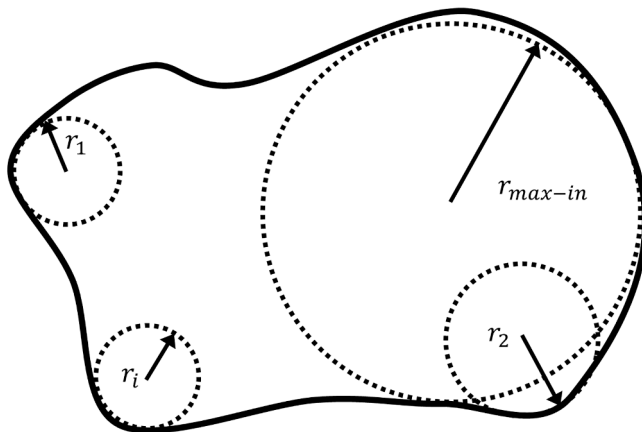
Fig. 2. The radii of particle corners r_i and the radius of the maximum inscribed sphere $r_{max\text{-}in}$ are used to calculate roundness *R*.

4. Networks

4.1. Network construction

Contact networks and *thermal* networks are constructed in this work to provide principles to design granular materials with superior force transmission and heat transfer. Since nodes in a contact network represent particle centroids, a first segmentation step is required to identify and label individual particles in the CT images (Fig. 1), for which the Otsu threshold (Otsu, 1979) segmentation is used to segment the solid and void phases in the packing. This is followed by the implementation of watershed segmentation (Legland et al., 2016, Zheng and Hryciw, 2016) to split the apparently "connected" solid phase into individual particles. The results after watershed segmentation of a local area in Ottawa sand is shown in Fig. 3 (a) and nodes are generated in the centres of particles. Edges in a contact network represent interparticle contacts which are detected if the particle boundary voxels are shared by

two neighbouring particles. CT images with smaller pixel-size may lead to a more accurate measurement of the interparticle contact area, but it compromises the sample size (would need to be smaller) and does not affect contact number significantly. By now, an unweighted contact network has been constructed since the edges only represent the connection of nodes. However, the edges in the unweighted contact network have the same capacity and cannot reflect the reality that the forces at interparticle contacts are not uniformly distributed. In fact, only a few particles/contacts carry most of the force transmission (Gan et al., 2017b, Antony et al., 2004). Therefore, each edge in the contact network is weighted by the interparticle contact area in this work. Here we draw a parallelism between force transmission and heat transfer, since heat mainly conducts through interparticle contacts in dry granular materials as well. The shared voxels detected after watershed segmentation are used to calculate the interparticle contact area with a greyscale intensity-based penalty factor to remove the overestimation introduced by partial volume effect (Wiebicke et al., 2017) following the framework in (Fei et al., 2019b). We build both unweighted contact networks to compute both *degree* (i.e., contact number or coordination number) and weighted contact networks to calculate *weighted degree* (combination of contact number and contact area) in this work. It will be later shown that heat transfer is influenced by interparticle contact area and number of contacts, and the use of network theory allow ready computation of variables (or features) that can account for both.

A *thermal* network is an extension of the *contact* network for the same sample. As shown in Fig. 3 (b), blue edges representing near-contacts are generated because heat also travel through the (small) inter-particle gaps due to the particle-void-particle heat conduction. Fig. 3 (c) shows the three dimensional (3D) thermal network for an ROI of Ottawa sand. Flatting interparticle contact points or changing gaps between neighbouring particle can change the solid–solid and solid-gap-solid heat transfer. In order to present the difference of the edges in thermal network acting as the heat transfer path, thermal conductance is assigned to each edge.

The thermal conductance of an edge indicates the capacity of heat transfer within particle *i*, through the interparticle contact/near-contact and into particle *j*. Hence, the thermal conductance of an edge C_{ij} is a combination of particle conductance C_i^p and C_j^p, interparticle contact conductance $C^{contact}$ and near-contact conductance C^{gap} using Eq.3.

$$C_{ij} = \left[\frac{1}{C_i^p} + \frac{1}{(C^{contact} + C^{gap})} + \frac{1}{C_j^p} \right]^{-1} \tag{3}$$

The three types of conductance were calculated using an equivalent particle cylinder (purple), an interparticle contact cylinder (orange) and a series of gap cylinders (light blue) as shown in Fig. 3 (b). Then, a general Eq. (4) can be used to compute the thermal conductance of individual cylinders.
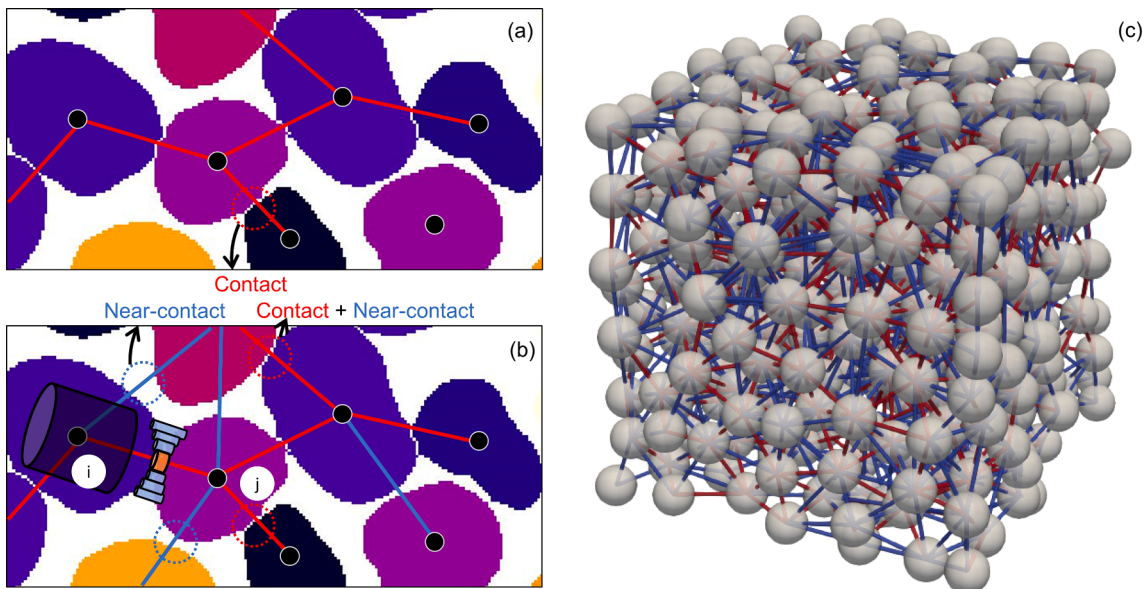
Fig. 3. Examples of the contact network and thermal network for the same sample. Contact edges are in blue (Fei and Narsilio, 2020a). (The reader is referred to the web version of this article for interpretation of the references to colour in this figure.) (For interpretation of the references to colour in this figure legend, the reader is referred to the web version of this article.)

$$C = \lambda \frac{A}{L} \qquad (4)$$

where C, λ A and L are the thermal conductance, thermal conductivity, cross-section area and length of a cylinder. Since this work focuses on dry sands under standard atmospheric pressure, the thermal conductivity of solid phase and air in the void space were set as 3 W/(mK) (Yun and Santamarina, 2008a, Yun and Evans, 2010, Sundberg et al., 2009) and 0.025 W/(mK) (Young et al., 1996) without considering the dependency on air pressure (Dai et al., 2017), respectively. Details of computing A and L for different types of cylinders can be found elsewhere (Fei et al., 2019b).

4.2. Network features

A network can be characterised at different length scales and these characteristics also vary over time due to compaction. This paper selects degree, edge betweenness centrality and global clustering coefficient because they can cover the diverse scales. As shown in Fig. 4 (a), particle A has the highest *degree* $\left[G^C\right]_\kappa$ which quantifies the relationship between particle A and its four neighbours. In complex network theory, *degree* is the feature defined as the number of edges for a node. In geotechnical engineering and material science this is known as *coordination number* in the case of a contact networks. After a deformation, from Fig. 4 (a) to Fig. 4 (b), particle B also has the largest degree but this variation can only be captured locally, not even by its neighbour particle

A. However, the variation can be reflected by the breakdown of the "square" into two "triangles" inter-particle connecting topology. The square and triangle are defined as *4-cycle* and *3-cycle* in complex network theory. A *l-cycle* in a network means a loop has *l* edges. The density of the triangles (3-cycles) can be measured using the *global clustering coefficient* G_{GC} as defined in Eq. (5) to trace the variation of microstructure across scales and time due to compaction.

$$G_{GC} = \frac{3 \times number\ of\ \text{closed triplets}}{number\ of\ \text{all triplets}} \qquad (5)$$

where a triplet is three nodes can either be connected by two edges (open triplet) or three edges (closed triplet).

Upon a further deformation from Fig. 4 (b) to Fig. 4 (c), particles are grouped into two clusters which are connected by an edge. This edge is essential for the force and heat transmission between the two clusters. The role of the edge acting as a "bridge" in complex network theory is captured as having the highest *edge betweenness centrality* $G_{B^{edge}}(e)$ in the network according to Eq. (6). In other words, the $G_{B^{edge}}(e)$ measures how important a given edge is in a network, which embodies the pathways for transmission of force or heat. In a global average sense when comparing different networks, higher average *edge betweenness centrality* $[G]_{B^{edge}}(e)$ means fewer edges with high importance in the network. However, fewer edges acting as pathways will lead to a less efficient transmission network in an unweighted network.
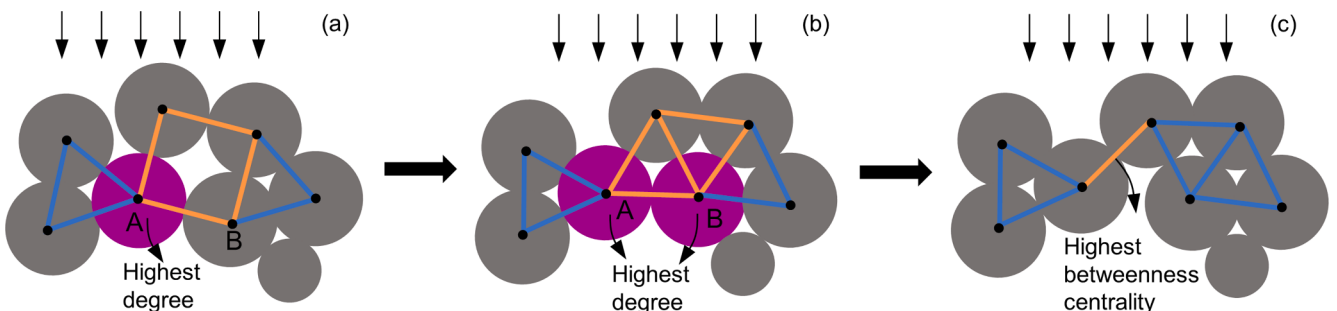
Fig. 4. Schematic network variation during compaction.

$$G_{B^{edge}}(\mathrm{e}) = \beta \sum_{j,k \in V} \frac{\sigma(j,k|\mathrm{e})}{\sigma(j,k)} \qquad (6)$$

where $\sigma(j,k)$ is the total number of shortest paths from node j to k, $\sigma(j,k|e)$ as the number of shortest paths from node j to k that overpass edge e. $\beta = 2/[|V|(|V|-1)]$ is a normalisation term.

Degree, edge betweenness centrality and *global clustering coefficient* covers three scales from the local particle scale to mesoscale (chain scale) and bulk scale. Degree and edge betweenness centrality are also computed for the weighted network since contact quality affects force and heat transmission. Global clustering coefficient is only calculated from the unweighted network to mainly quantify the structural variation under compaction.

5. Results

For each sand, four ROIs are selected from different locations for computing particle shape descriptors and the three selected network features. The involvement of the four ROIs could mitigate the impact of the potential heterogeneity on the microstructural parameters.

5.1. Sphericity and roundness

Fig. 5 (a) shows the distribution of sphericity of grains in the three selected sands. According to Eqs. (1) and (2) for calculating sphericity and roundness, the range of both sphericity and roundness are between zero and one. For each obtained distribution, a normal distribution curve is fitted so its peak represents the average sphericity of each sand sample. The peaks of the normal distribution curves for sphericity move left from Glass beads to Angular sand, which means the average sphericity decreases when grains in sands become more irregular. Glass beads made of the most round particles have the largest average sphericity almost reaching one with a narrow span. In contrast, the Angular sand consisting of the most irregular particles has the smallest average sphericity despite a wide span ranging from 0.4 to 0.6.

Similarly, the peak of the distribution curve for roundness in Fig. 5 (b) also moves left from Glass beads to Angular sand. Hence, the average
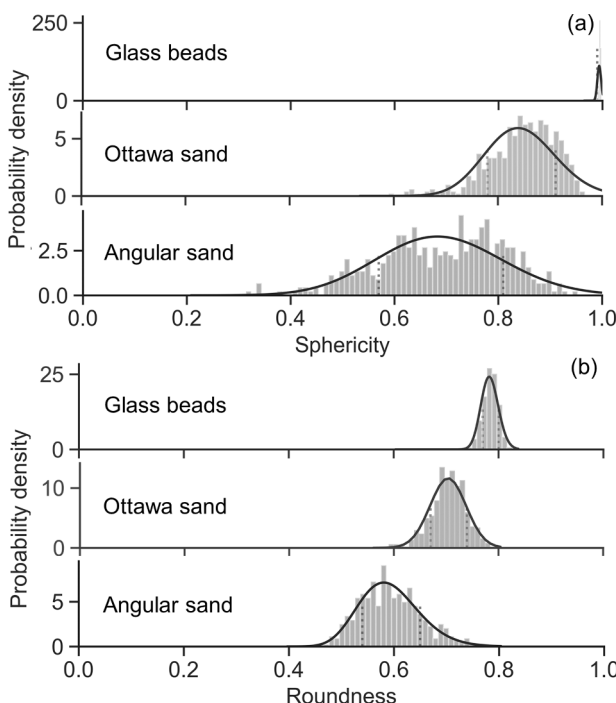
Fig. 5. Distributions of sphericity S (a) and roundness R (b) of particles in three sands.

roundness is also smaller in a sand composing of more irregular particles in this case. The span of the roundness in Glass beads is broader than that of sphericity while it is narrower in Ottawa sand and Angular sand. Only using either sphericity and roundness cannot capture the particle shape of all irregular sands grains since the sphericity indicate the particle shape at the particle scale while the roundness focuses on the descriptions of grain corners (Fei et al., 2019a). For the sands in this work, the both sphericity and roundness decrease from round Glass beads to Angular sand. However, this sphericity and roundness correlation may be different for a more general case and when a larger range of particle shapes are analysed by introducing other sands. Therefore, an average of sphericity (S) and roundness (R) is defined here and noted as *SR* to quantify the (individual) particle shape of the three sands in this paper:

$$SR = \frac{S+R}{2} \qquad (7)$$

The mean of average sphericity and average roundness SR_{ave} is used to characterise and quantify the particle shape of samples (collection of individual particles) in this paper, we note however that the results presented in the following sections and trends observed for SR_{ave} will still hold as function of only S or only R for the samples analysed here:

$$SR_{ave} = \mathrm{average(SR)} \qquad (8)$$

5.2. Impact of particle shape on degree

The degree in a network measures the number of edges for a node. Hence, the physical meaning of degree in a contact network is the number of neighbouring particles that a target particle is in contact with: it is widely known in geotechnical engineering as the coordination number. Since the boundary particles on the subsamples are not wholly presented in Fig. 1, they are excluded from the statistics of the network features. Fig. 6 (a) shows that the average degree $\left[G^C\right]_\kappa$ from the contact network increases with the increase of SR_{ave} (the average SR in a given sample) when no loading is applied. In other words, irregular particle packings show smaller average coordination number than in round particle packings. The relatively small average degree (coordination number) in Angular sands is attributed to factors such as the particle alignment and interlocking (Delaney and Cleary, 2010).

The average degree in each sand increases when the sample is subjected to a larger axial compressive loading. The first loading stage (0–2.0 MPa) contributes the largest degree variation which is around twice as the total variation in the following two stages (2.0–10.2 MPa). It is noticeable that SR_{ave} fluctuates slightly in Fig. 6 due to particle breakage under compression. During the whole loading period, the average degree in Ottawa sand and Angular sand experiences a larger variation than that in Glass beads, indicating that the variation of the average coordination number in irregular sand may be more sensitive to loadings. After applying 10.2 MPa to the three sands, it is noteworthy that the $\left[G^C\right]_\kappa$ in Ottawa sand reaches a high value that is larger than that in either the roundest Glass beads or Angular sand which has the most complex particle shape (Fig. 1). Fig. 1 (b) shows that Ottawa sand has particles such as particle A with round shapes while also has some elongated particles such as particle B. The elongated particles with the same initial coordination number as spheres due to the particle alignment have more potential freedom to rotate. As shown in Fig. 7 (a-b), the central sphere A can be trapped by three neighbours while eclipse Fig. 7 (c-d) can escape the trap when its neighbours have small displacements. This also contributes to the large variation of $\left[G^C\right]_\kappa$ in Ottawa sand and Angular sand during the first loading stage. As the loading increases further, the rotation of particles in Angular sand becomes frustrated because of the local concaves in their surface which induce interlocking as shown in Fig. 7 (e-f).

The restriction of rotation in Angular sand is also depicted in the bivariate Kernel Density Estimation (KDE) distributions shown in Fig. 8
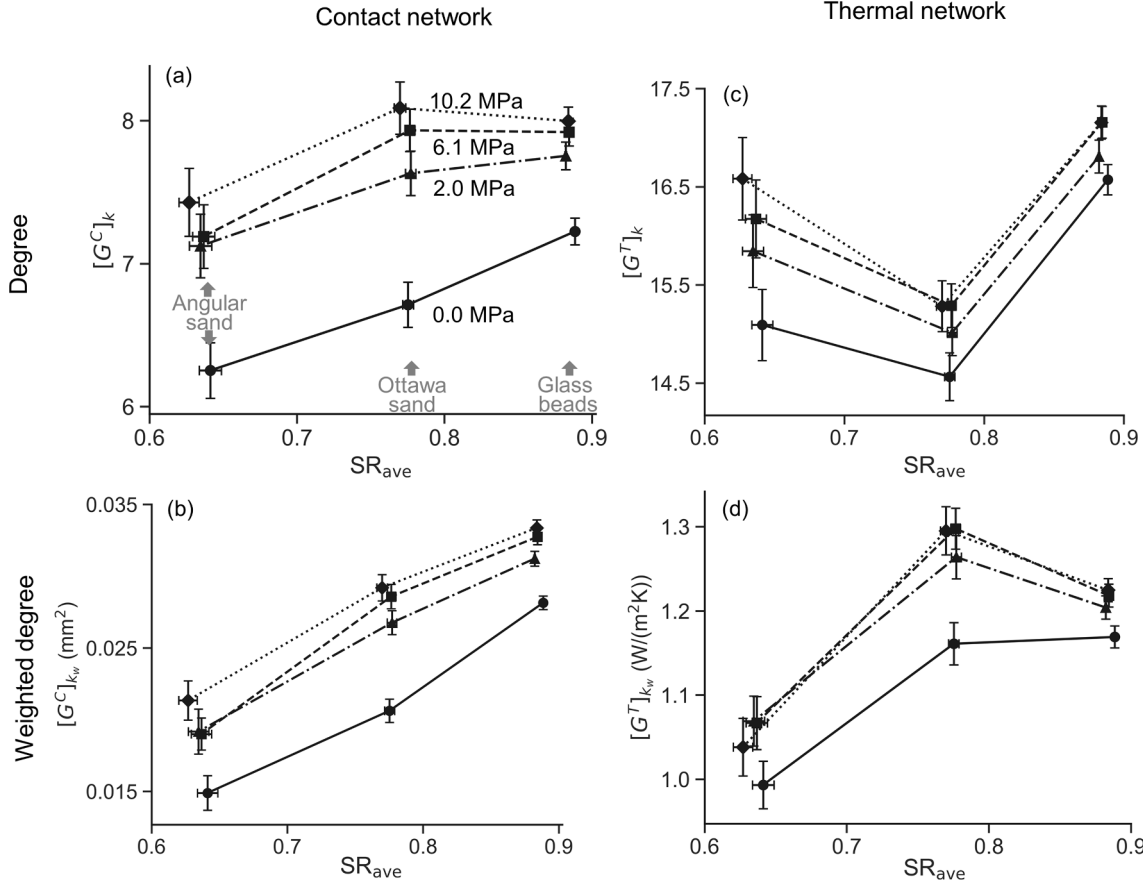
Fig. 6. Impact of particle shape on the average degree. The error bar shows the 95% confidence interval calculated on network nodes or edges of the combined set of the four ROIs.
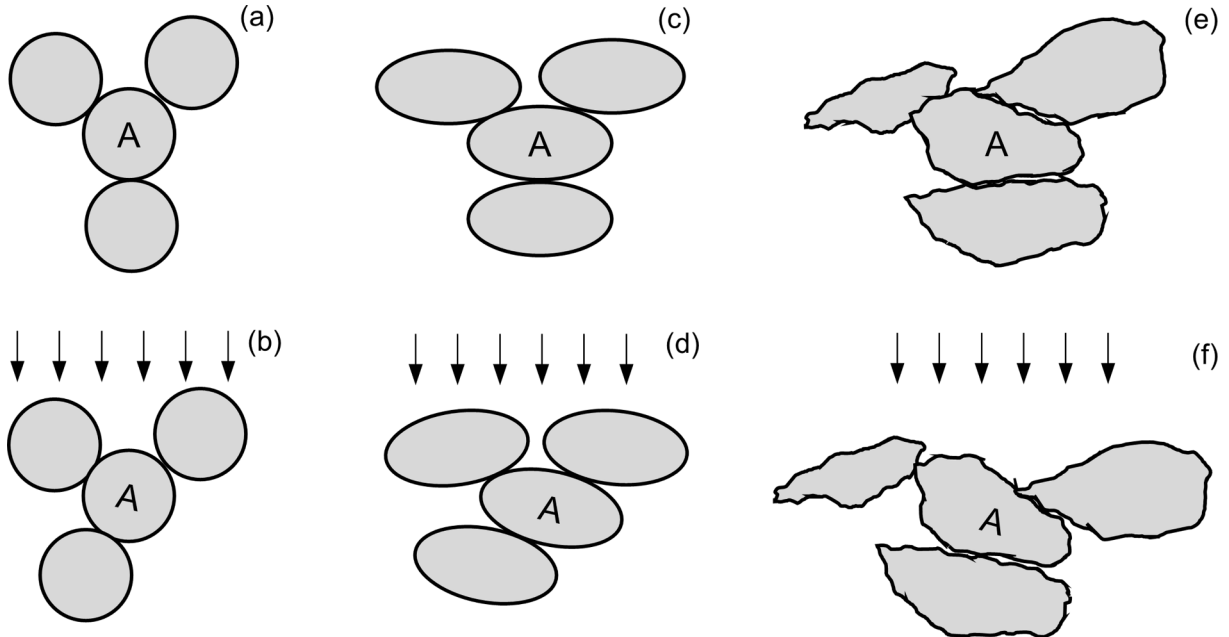
Fig. 7. Schematic illustration of particle movement.

(a-b). The histograms used to generate the KDE curves can be found in Appendix A. The KDE curve in the very left of Fig. 8 (a) has a straight vertical boundary corresponding the most irregular particles with G_κ^C between 5 and 10 when the sample is under no loading. Those irregular particles keep their G_κ^C at 5–10 under 10.2 MPa axial stress, forming a lump at the left of Fig. 8 (b). However, irregular particles in Ottawa sand are smoother with rare concaves so that their coordination number or degree can still increase under high loadings. Hence, the G_κ^C on the left
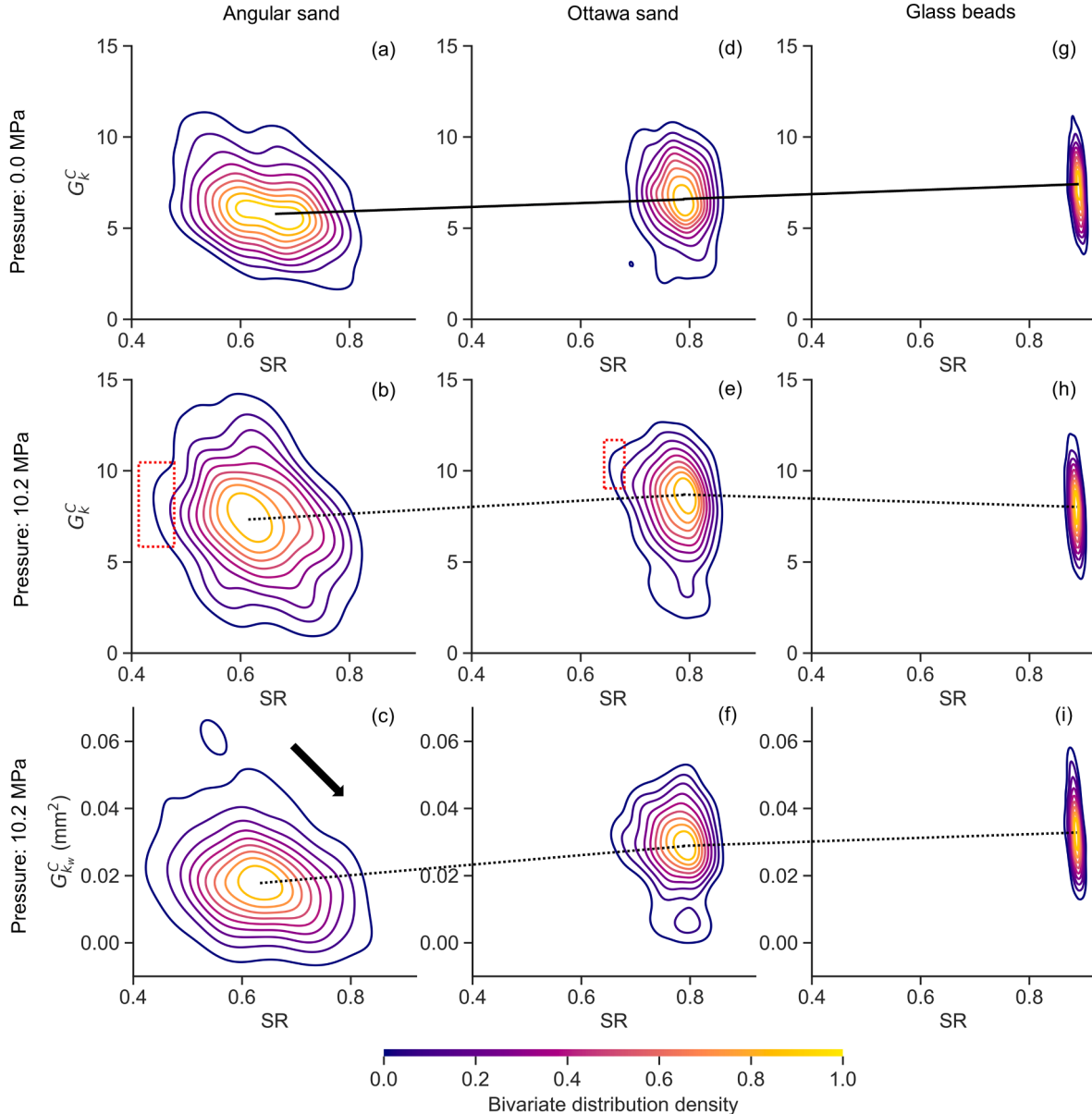
Fig. 8. Kernel density estimation (KDE) of unweighted/weighted degree in contact network under different stress. The first and second row show the KDE of unweighted degree under 0 and 10.2 MPa pressure, respectively. The bottom row shows the KDE of weighted degree under 10.2 MPa. (The reader is referred to the web version of this article for interpretation of the references to colour in this figure.)

boundary in Fig. 8 (e) increases compared with that in Fig. 8 (d). Ottawa sand with moderate particle irregularity has lower $\left[G^C\right]_\kappa$ than Glass beads under no loading but then larger than Glass beads under high pressure, which implies that there may be a transient state when the effect of SR_{ave} on average coordination number turns from positive to negative. Furthermore, the KDE curve in Fig. 8 (a) shows that more irregular particles have higher G_κ^C, this trend is opposite to that of its mean value $\left[G^C\right]_\kappa$. The opposite trend also indicates the existence of the transient state.

Network edges can be weighted to suit specific applications, resulting in more informative weighted network features since the new features consider not only the network topology but also the weight at network edges. In this work, contact network edges are weighted by the interparticle contact area since it is another essential factor to heat and

mechanical transmission apart from particle connectivity (Yun and Santamarina, 2008b, Walker and Tordesillas, 2010). After weighting the contact network, the variation of weighted degree $\left[G^C\right]_{\kappa_w}$ due to loadings in all sands becomes smaller shown in Fig. 6 (b) compared with the variation in Fig. 6 (a). The error bars of $\left[G^C\right]_{\kappa_w}$ are also shorter than that of $\left[G^C\right]_\kappa$, indicating the $\left[G^C\right]_{\kappa_w}$ more like an invariant. Additionally, $\left[G^C\right]_{\kappa_w}$ in Glass beads at all loading stages presents the largest value in contrast with the unweighted $\left[G^C\right]_\kappa$ in Ottawa sand is largest under 10.2 MPa loading. The consistent positive correlation between $\left[G^C\right]_{\kappa_w}$ and SR_{ave} indicates the importance of considering both contact number and contact quality when characterising microstructure in granular materials. After weighting the contact network edges with contact area, the KDE shape in Fig. 8 (b) becomes flat in Fig. 8 (c) although a small

separated circle at the top left. The KDE shape of Ottawa sand in Fig. 8 (e) also becomes flat in Fig. 8 (f), the left bound related to irregular particles has a big sink although the change of the general shape of the KDE is more gentle than that in Angular sand.

A thermal network is an extension of the contact network by further considering near-contacts, so that the degree from the thermal network becomes the total number of interparticle contact and near-contacts. Fig. 6 (c) shows that the relationship between SR_{ave} and the average degree $[G^T]_\kappa$ from thermal network has a valley at Ottawa sand rather than a small hump in Fig. 6 (a). The difference between the degree in thermal network and contact network is the number of near-contacts. By comparing the degree value in Fig. 6 (a) and (c), it can be seen that Glass beads and Angular sand have a similar amount of near-contacts around nine per particle, while Ottawa sand has fewer than eight per particle. The range of G^C_κ of Angular sand and Ottawa sand shown in Fig. 8 (b) and (e) are similar. In contrast, in thermal networks, Fig. 9 (a) and (c) shows the frequency of thermal network feature G^T_κ in Ottawa sand is mainly between 10 and 22. The lower bound of 10 in this main part is same as the minimum in Glass beads in Fig. 9 (e) but the upper bound in Ottawa sand is smaller than that in Glass beads, 22 versus 27 (Appendix A), respectively. Moreover, the bottom part in Fig. 9 (c) further reduces the average G^T_κ in Ottawa sand, resulting in the valley in Fig. 6 (c).

Since edges in a thermal network correspond to the heat transfer paths, thermal conductance is assigned to each edge representing either interparticle contact or near-contact. After considering the edge capacity, Fig. 6 (d) shows that the thermal network weighted degree $[G^T]_{\kappa_w}$ in Ottawa sand become the peaks when loading is above 2.0 MPa, which is similar to $[G^C]_\kappa$ in Fig. 6 (a) and lines in Fig. 6 (d) are closer. The similarities are because interparticle contacts have much larger thermal

conductance than that of near-contacts in dry sands. Since Ottawa sand has a smaller amount of near-contacts, weighting interparticle contacts by thermal conductance results in turning the value of Ottawa sand from valleys in Fig. 6 (c) to peaks in Fig. 6 (d). After considering thermal conductance at each edge in the thermal network, Fig. 9 (b) has a similar shape to Fig. 9 (a) but a more obvious corner at bottom right, indicating that irregular particles have both more thermal edges and thermal conductance. In contrast, some particles in Ottawa sand with $SR = 0.8$ have largest thermal conductance, stretching the upper part of KDE shape from circles in Fig. 9 (c) to ovals in Fig. 9 (d).

The average weighted degree $[G^C]_{\kappa_w}$ has a consistently increasing trend with the increase of SR_{ave} in Fig. 6 (c). However, focusing on individual particles instead of the whole sample, the effect of SR on $G^C_{\kappa_w}$, in Fig. 8 (c) in particular, has a decreasing trend. In a natural sand, the particles have different particle size, which cannot be controlled as using Discrete Element Method (DEM) to generate particles in the same equivalent particle size (D_{eq}) (Zhao et al., 2017). Hence, an analysis of how particle shape affects $G^C_{\kappa_w}$ while isolating the effect of particle size is conducted. The interplay among SR, D_{eq} and $G^C_{\kappa_w}$ of particles from a ROI in each sand is present in Fig. 10 (a-c). The colour of the datapoints becomes lighter from left to right, indicating D_{eq} plays a positive role to $G^C_{\kappa_w}$. Additionally, for a given D_{eq} (dash line) in each sand, $G^C_{\kappa_w}$ has a subtle increase from top to bottom, which is same as the trend that irregular particles have larger $G^C_{\kappa_w}$ observed from Fig. 8. The combined impact of D_{eq} and SR controls the dot colour has a general brighten trend from top left to bottom right, most obvious in Glass beads. As for the weighted degree $G^T_{\kappa_w}$ from the thermal network, its relationship with SR and D_{eq} is presented in Fig. 10 (d-f). Some light datapoints in the red box
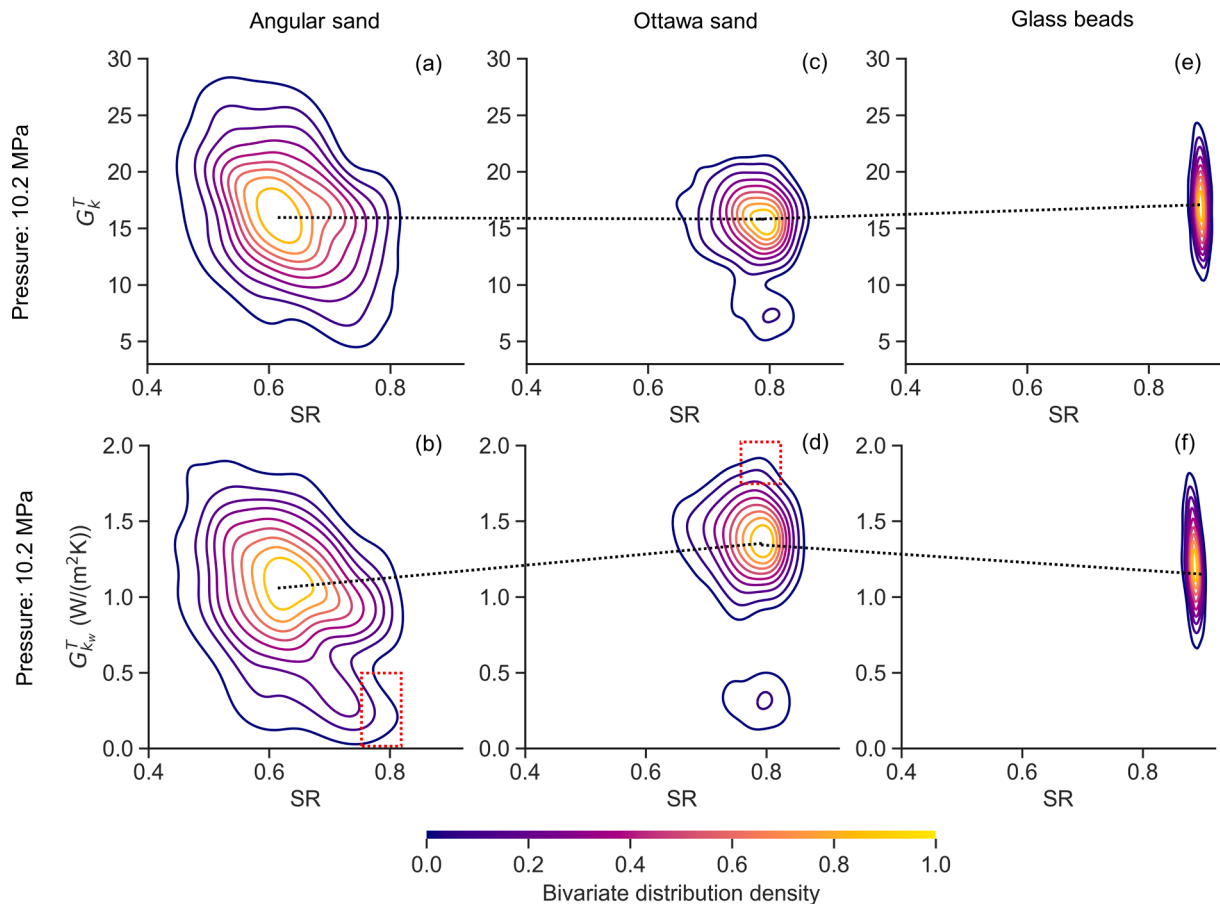
Fig. 9. Kernel density estimation (KDE) of degree in thermal network. The first row shows the KDE of unweighted degree while the second rows shows the weighted degree 10.2 MPa pressure. (The reader is referred to the web version of this article for interpretation of the references to colour in this figure.)
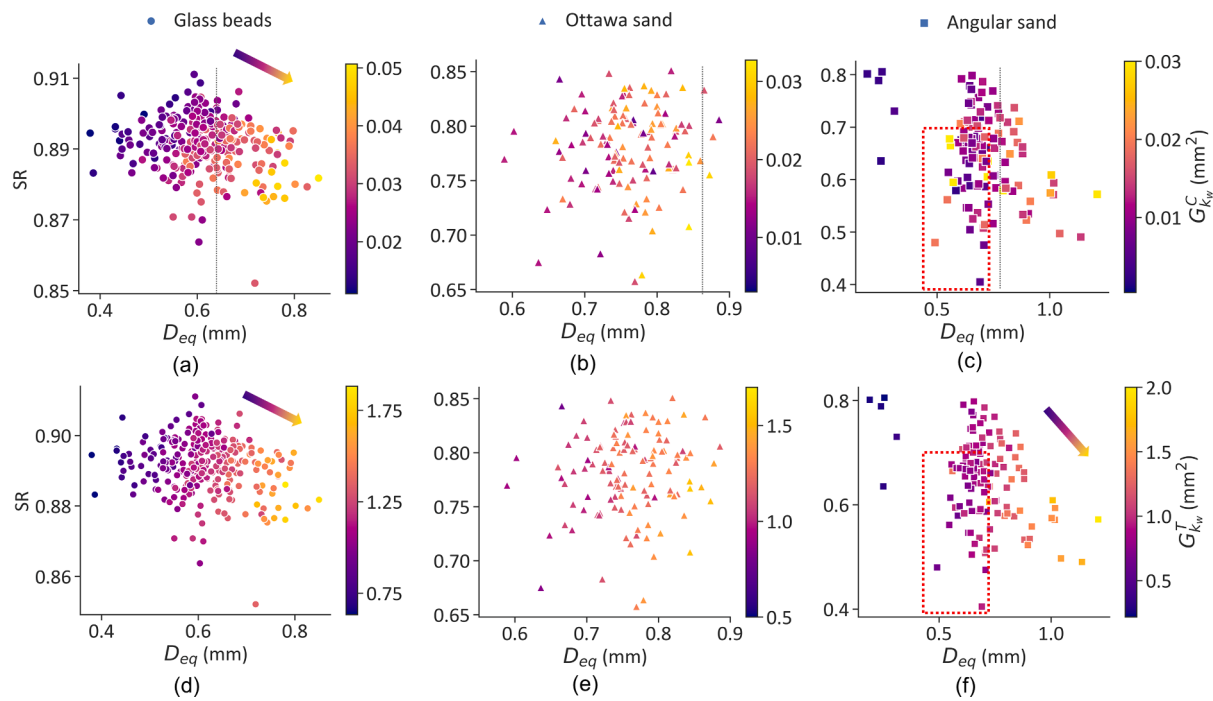
Fig. 10. A ROI is selected from each sand under no loading, the interplay among particle shape SR, equivalent diameter D_{eq} and weighted degree $G^C_{\kappa_w}$. The figures in the first row are coloured by weighted degree from contact network $G^C_{\kappa_w}$ (a, b, c) while the figures in the second row are coloured by weighted degree from thermal network $G^T_{\kappa_w}$ (d, e ,f). (The reader is referred to the web version of this article for interpretation of the references to colour in this figure.)
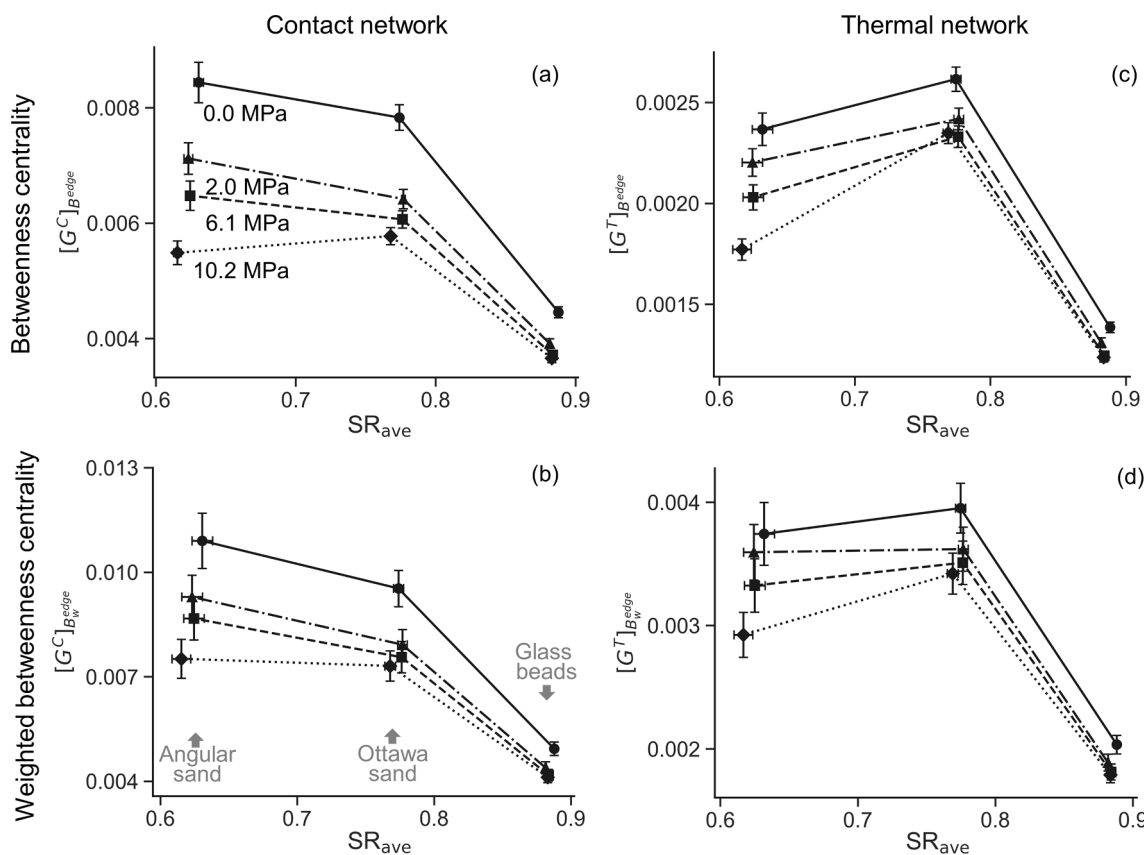
Fig. 11. Impact of particle shape on edge betweenness centrality. The error bar shows the 95% confidence interval calculated on network nodes or edges of the combined set of the four ROIs.

of Fig. 10 (c) turn into dark in Fig. 10 (f), which makes the general brighten trend of a weighted degree from top left to right bottom more obvious. The same enhancement of the trend is also found in Fig. 10 (e) compared with Fig. 10 (b). These findings prove again that the impact of particle shape on the average degree of a sand sample is different from the impact for individual grains within the sand sample.

5.3. Impact of particle shape on edge betweenness centrality

The degree focuses on a local neighbourhood of a node and does not consider other nodes far from a grain's immediate neighbourhood since grains away from it cannot be reached directly. *Edge betweenness centrality*, on the other hand, can help characterise the topology in this "long"-distance since it quantifies the importance of an edge relative to all the other edges in the whole network. This network feature, from a physics point of view, is directly related to the preferred force and heat transfer path since edges in a contact network corresponds to interparticle contacts and edges in a thermal network are related to solid–solid or solid-void-solid heat transfer. *SR* characterises the morphology of a particle while *edge betweenness centrality* quantifies interactions between particles. Hence, the average *SR* of the particles that the edge connects is used to evaluate the impact of particle shape on *edge betweenness centrality*.

Fig. 11 (a) shows that the average edge betweenness centrality $\left[G^C\right]_{B^{edge}}$ of the contact networks decreases as average particle shape descriptor SR_{ave} increases. This negative impact of particle shape on $\left[G^C\right]_{B^{edge}}$ is opposite to the positive impact on $\left[G^C\right]_K$ in Fig. 6 (a). Irregular particle packings tend to have high edge betweenness centrality because clusters are more isolated in them so that some edges are more important to connect different clusters as illustrated in Fig. 4 (c). The $\left[G^C\right]_{B^{edge}}$ also decreases when a higher axial loading is applied to the sand sample. The variation of $\left[G^C\right]_{B^{edge}}$ in the more irregular sand is bigger, making the $\left[G^C\right]_{B^{edge}}$ of Angular sand even smaller than that of Ottawa sand under 10.2 MPa loading. From the histograms in the first column of Appendix B, fewer particles have high $G^C_{B^{edge}}$ while more particles have small $G^C_{B^{edge}}$.

After weighting the edges of contact network by interparticle contact area, some edges play a more crucial role as "bridges" with high weighted edge betweenness centrality $G^C_{B^{edge}_w}$ indicated by the long tail in the second column of Appendix B. Particles in natural dry sand touch each other instead of floating due to the gravity. Hence, each particle has a non-zero degree but the edge betweenness centrality corresponding to an interparticle contact could be zero if no shortest path passes through the contact. Edges in a weighted network are more prone to have zero edge betweenness centrality as shown in the second column of Appendix B and can reveal the truth that most of the contacts carry small forces (e. g., arching effect) while only a small amount of contacts transmit most of the large forces (e.g., force chain). As for the average weighted edge betweenness centrality $\left[G^C\right]_{B^{edge}_w}$, its negative relationship with SR_{ave} in Fig. 11 (b) is similar to that before weighting the contact network in Fig. 11 (a). The similarity hints that using edge betweenness centrality to study the impact of particle shape on microstructure could save the extra work of weighting networks.

The impact of particle shape on average edge betweenness centrality in unweighted and weighted thermal networks also share a similar relationship according to Fig. 11 (c-d) even though Ottawa sand has peak values. Weighted $\left[G^T\right]_{B^{edge}_w}$ is larger than unweighted $\left[G^T\right]_{B^{edge}}$ similar to that in contact network. Additionally, the last column of Appendix B shows more edges have zero $G^T_{B^{edge}_w}$ than that in contact network

due to the near-contacts in the weighted thermal network have small thermal conductance.

Since edges in a contact network are related to force transmission and edges in a thermal network corresponds to heat transfer, the correlation of *weighted edge betweenness centrality* to the particular physical process renders values associated to these processes. This work only studies the correlation of $G^T_{B^{edge}_w}$ to heat transfer due to the difficulty of calculating the force at contacts in a real natural sand sample experimentally. The heat flux at each edge is calculated by substituting thermal conductance into Fourier's law (Fei et al., 2019b). The histograms of heat flux in Glass beads, Ottawa sand and Angular sands under loadings are presented in Fig. 12 (a-c). The distributions show a high frequency of low values on the left and long tails on the right, which is similar to the distribution of weighted edge betweenness centrality in the second and fourth columns of Appendix B. In contrast, the weighted degree in Appendix A presents a kind of normal distribution. Therefore, *weighted edge betweenness centrality* is a network feature better suited to the study of heat transfer.

The long tail in histograms of heat flux in Fig. 12 (a-c) also indicates that a small amount of edges dominates heat transfer in dry sands. To quantify the domination, the cumulative histograms of heat flux are plotted on the top of Fig. 12 (d-f) under which the cumulative percentage of the sum of heat transfer in each bin out of the total heat flux of all edges are plotted. An identical observation in all cases for distinct sands and under different loading in Fig. 12 (d-f) is that 20% edges (above 0.8) are responsible for the 60% (above 0.4) heat transfer. This further emphasises the importance of studying the role of edges, such as using edge betweenness centrality herein.

Since weighted edge betweenness centrality has a similar distribution as heat flux, its relationship with particle shape for individual edges is visualised in Fig. 13 with the consideration of singling out the impact of equivalent particle diameter D_{eq}. Similar to the interplay between weighted degree, SR and D_{eq} in Fig. 10, Fig. 13 also shows a general trend that the value of the various contact network features increases from the top left to the bottom right (see colour bar distribution legend). The figures in the second row represent thermal network results, showing more datapoints than that of contact networks in the first row because they correspond to near-contacts which have small $G^T_{B^{edge}_w}$. The trend indicates that particle irregularity boosts a larger edge betweenness centrality, which is same as the relationship between the average particle shape descriptor SR_{ave} and average weighted edge betweenness centrality $\left[G^C\right]_{B^{edge}_w}$ at the sample scale. This consistent relationship at both particle scale and sample (bulk) scale depicts the merit of implementing edge betweenness centrality to study the microstructure of granular materials over weighted degree.

5.4. Impact of particle shape on global clustering coefficient

The global clustering coefficient is a macro-scale microstructure which describes the extent to which the particles are clustered together. The global clustering coefficient G^C_{GC} from a contact network also hints the rigidity of a sample since it quantifies the density of triples (triangles) which tend to restrict deformation according to rigidity theory (Thorpe and Duxbury, 1999), even in 3D analysis (Rivier, 2006, Baram et al., 2004). It can be seen from Fig. 14 (a) that round Glass beads have the largest G^C_{GC} since they have large coordination number (Fig. 6 (a)). Although the global clustering coefficient G^T_{GC} from the thermal network considers extra edges related to near contacts and Ottawa sand has fewer edges than Angular sand, Fig. 14 (b) also shows that G^T_{GC} has a general increase when sands are more regular. Moreover, Fig. 14 (c) presents
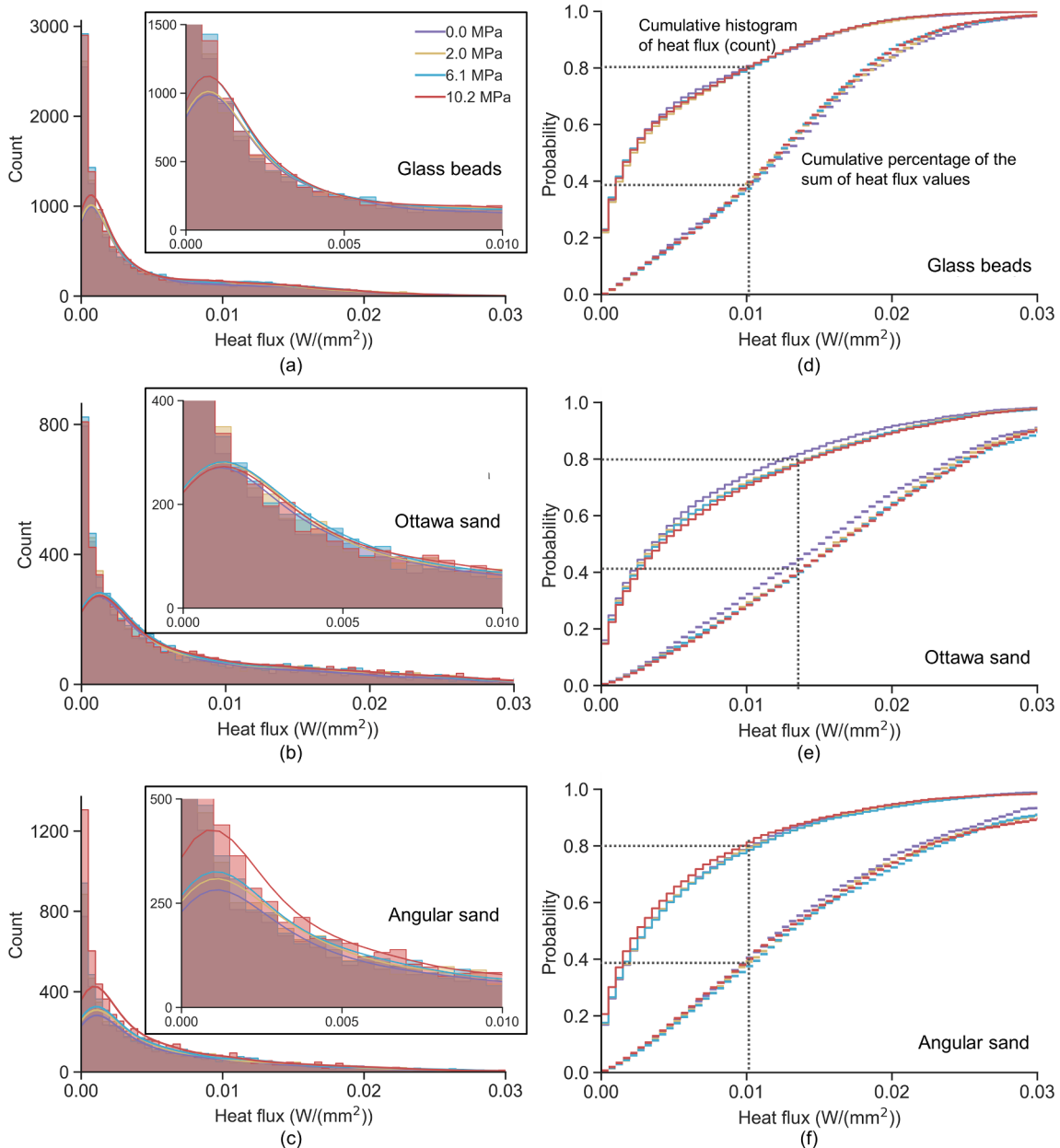
Fig. 12. Heat flux: The left column shows the histogram of heat flux across edges in three sands, the top right box in each figure is a magnification. The right column presents the cumulative histogram of heat flux (top stepping lines) and cumulative percentage of the sum of heat flux in each bin over the total heat flux (bottom short horizontal lines). (The reader is referred to the web version of this article for interpretation of the references to colour in this figure.)

that G_{GC}^T keep increasing when more loading is added to the samples, indicating that G_{GC}^T has a good correlation with the rigidity of the samples. Hence, the slopes of lines in Fig. 14 (d), which present the impact of particle shape on effective thermal conductivity (calculated using thermal conductance network model in (Fei et al., 2019b)) under loadings are similar to the slopes of the lines in Fig. 14 (b).

6. Conclusion

We investigated the impact of particle shape on the microstructure of granular materials in light of mechanical strength and heat transfer. This is achieved by characterising the contact networks and thermal networks of three sands, using different network features: degree, edge

betweenness centrality and global clustering coefficient. The edges are weighted by the interparticle contact area in the contact networks, and by the thermal conductance in the thermal networks. An assessment of the impact of particle shape is performed at two levels: individual particles and the whole sample.

At the level of individual particles, we found that 60% of heat transfer is carried by 20% of the edges in all three sands under different loadings. These few edges as important pathways for heat transfer have high weighted edge betweenness centrality. At the sample scale, higher *average* unweighted edge betweenness centrality exists in a more irregular-shaped particle packing, indicating the sample has fewer heat pathways and results in a less efficient transmission network. Therefore, edge betweenness centrality is a good candidate to characterise the
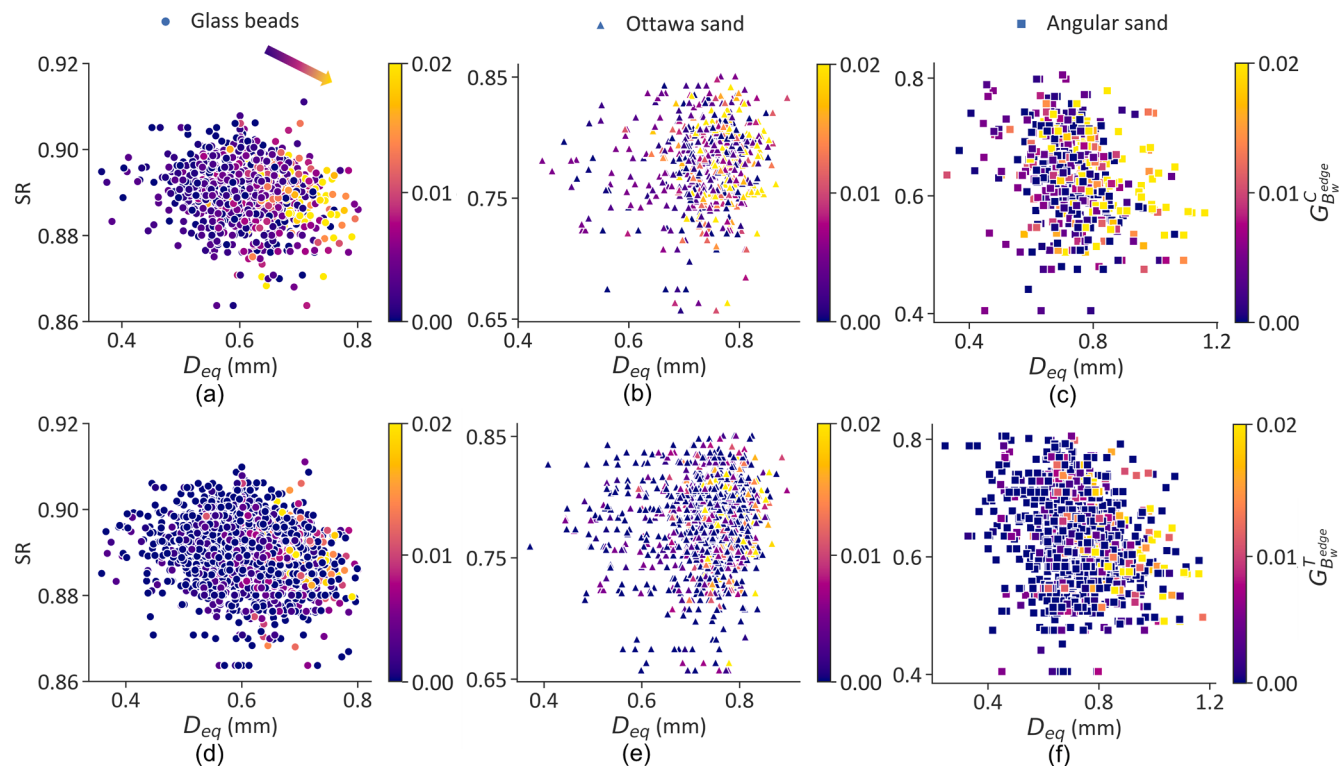
Fig. 13. A ROI is selected from each sand, the interplay among particle shape SR, equivalent diameter D_{eq} and weighted edge betweenness centrality. The figures in the first row are results from contact network (a, b, c) while the figures in the second row are results from thermal network (d, e, f). (The reader is referred to the web version of this article for interpretation of the references to colour in this figure.)
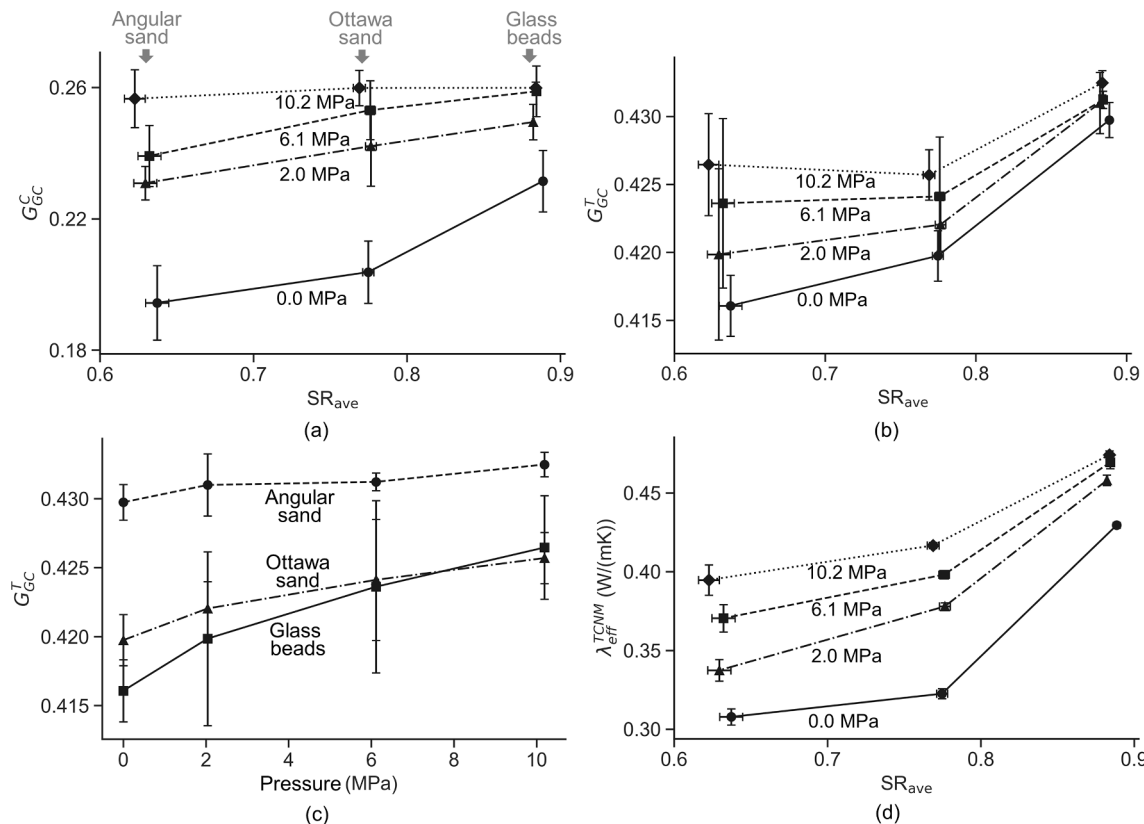
Fig. 14. Impact of particle shape on global clustering coefficient from contact networks (a) and that from thermal networks (b). Relationship between loading and global clustering coefficient from the thermal network is shown in (c). The impact of particle shape on effective thermal conductivity is shown in (d). The error bar shows the 95% confidence interval calculated on network nodes or edges of the combined set of the four ROIs.

microstructure of granular materials for the study of force and heat transfer. The impact of particle shape on the *average* edge betweenness centrality has a similar relationship for unweighted and weighted networks in the three sands. Hence, in this context, the use of an unweighted network is sufficient and offers the advantage of a significant saving on computational time.

While comparing the degree G_κ^C of individual particles in a given sample, irregular particles have larger G_κ^C than round particles. If focusing on comparing the sample-scale *average* degree $\left[G^C\right]_\kappa$ in different sands, an opposite trend is observed: sand made of irregular particles has smaller $\left[G^C\right]_\kappa$ under different loadings due to particle alignment and interlocking. This trend is even more obvious for the average weighted degree $\left[G^C\right]_{\kappa_w}$.

Global clustering coefficient is a sample-scale feature. Round particle assemblies tend to have higher global clustering coefficient in both the contact network and thermal network. Additionally, the global clustering coefficient also increases with the increase of compaction, indicating that the global clustering coefficient from thermal network G_{GC}^T can also hint at the rigidity of sands. Finally, the impact of particle shape on G_{GC}^T is similar to the impact of particle shape on effective thermal conductivity.

CRediT authorship contribution statement

Wenbin Fei: Conceptualization, Methodology, Investigation, Validation, Formal analysis, Data curation, Writing - original draft, Visualization, Funding acquisition. **Guillermo A. Narsilio:** Conceptualization, Methodology, Resources, Writing - review & editing, Funding acquisition. **Joost H. van der Linden:** Methodology, Writing - review & editing. **Antoinette Tordesillas:** Methodology, Writing - review & editing. **Mahdi M. Disfani:** Resources, Writing - review & editing, Funding acquisition. **J. Carlos Santamarina:** Conceptualization, Methodology, Funding acquisition.
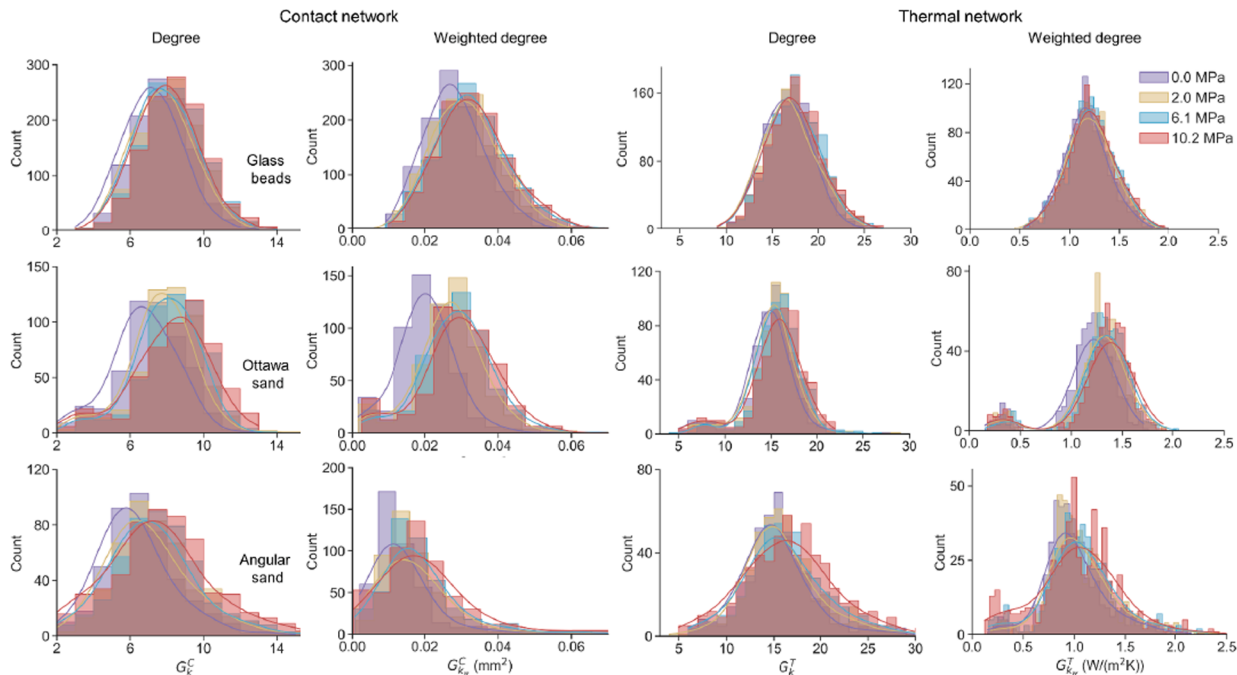
Declaration of Competing Interest

The authors declare that they have no known competing financial interests or personal relationships that could have appeared to influence the work reported in this paper.

Acknowledgements
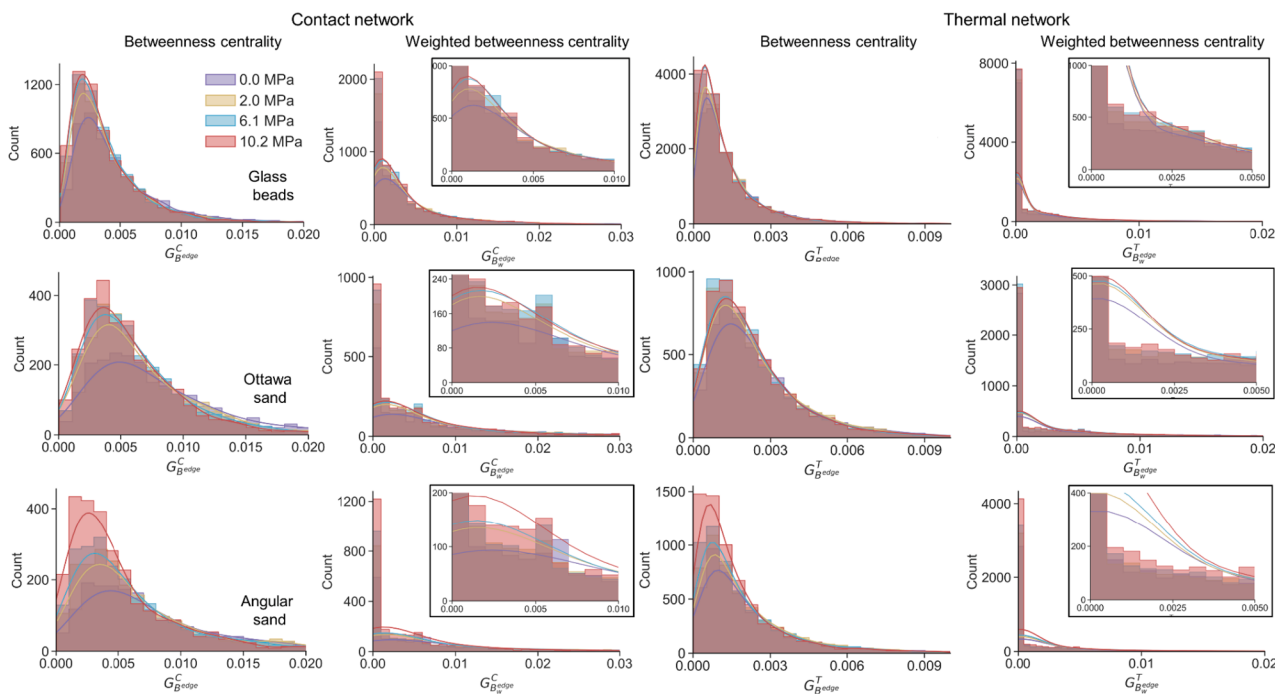
Appendix A

The rows from top to bottom are results related to Glass beads, Ottawa sand and Angular sand. The columns from left to right show the histogram of unweighted degree from contact network, weighted degree from contact network, unweighted degree from thermal network and weighted degree from thermal network. (The reader is referred to the web version of this article for interpretation of the references to colour in this figure.)

Appendix B

The rows from top to bottom are results related to Glass beads, Ottawa sand and Angular sand. The columns from left to right show the histogram of unweighted edge betweenness centrality from contact network, weighted edge betweenness centrality from contact network, unweighted edge betweenness centrality from thermal network and weighted edge betweenness centrality from thermal network. The box in some figures are magnifications. (The reader is referred to the web version of this article for interpretation of the references to colour in this figure.)

References

Antony, S.J., Kuhn, M.R., 2004. Influence of particle shape on granular contact signatures and shear strength: new insights from simulations. Int. J. Solids Struct. 41 (21), 5863–5870.

Astm, 2017. C778-17 standard specification for standard sand. ASTM International, West Conshohocken, PA.

Baram, R.M., Herrmann, H., Rivier, N., 2004. Space-filling bearings in three dimensions. Phys. Rev. Lett. 92 (4), 044301.

Birkholz, O., Gan, Y., Kamlah, M., 2019. Modeling the effective conductivity of the solid and the pore phase in granular materials using resistor networks. Powder Technol. 351, 54–65.

Brocato, M., 2020. A continuum model of close packing granular materials for the study of rock filled gabions. Int. J. Solids Struct. 187, 38–47.

Chari, V.D., Sharma, D.V., Prasad, P.S., Murthy, S.R., 2013. Dependence of thermal conductivity in micro to nano silica. Bull. Mater. Sci. 36 (4), 517–520.

Cho, G.-C., Dodds, J., Santamarina, J.C., 2006. Particle Shape Effects on Packing Density, Stiffness, and Strength: Natural and Crushed Sands 132(5), 591–602.

Dai, W., Hanaor, D., Gan, Y., 2019. The effects of packing structure on the effective thermal conductivity of granular media: A grain scale investigation International. Journal of Thermal Sciences 142, 266–279.

Dai, W., Pupeschi, S., Hanaor, D., Gan, Y., 2017. Influence of gas pressure on the effective thermal conductivity of ceramic breeder pebble beds. Fusion Eng. Des. 118, 45–51.

Delaney, G.W., Cleary, P.W., 2010. The packing properties of superellipsoids. EPL (Europhysics Letters) 89 (3), 34002.

Fei, W., Narsilio, G.A., 2020a. Impact of Three-Dimensional Sphericity and Roundness on Coordination Number. J. Geotech. Geoenviron. Eng. 146 (12), 06020025.

Fei, W., Narsilio, G.A., 2020b. Network analysis of heat transfer in sands. Comput. Geotech. 127, 103773.

Fei, W., Narsilio, G.A., 2021. XCT images and networks of Ottawa sand and Angular sand. Mendeley Data.

Fei, W., Narsilio, G.A., Disfani, M.M., 2019a. Impact of three-dimensional sphericity and roundness on heat transfer in granular materials. Powder Technol. 355, 770–781.

Fei, W., Narsilio, G.A., Van Der Linden, J.H., Disfani, M.M., 2019b. Quantifying the impact of rigid interparticle structures on heat transfer in granular materials using networks. Int. J. Heat Mass Transf. 143, 118514.

Fei, W., Narsilio, G.A., Van Der Linden, J.H., Disfani, M.M., 2020. Network analysis of heat transfer in sphere packings. Powder Technol. 362, 790–804.

Fei, W., Narsilio, G.A., Van Der Linden, J.H., Disfani, M.M., Miao, X., Yang, B., Ashfar, T., 2021. X-ray computed tomography images and network data of sands under compression. Data in Brief (in press).

Gan, J., Zhou, Z., Yu, A., 2017a. Effect of particle shape and size on effective thermal conductivity of packed beds. Powder Technol. 311, 157–166.

Gan, J., Zhou, Z., Yu, A., 2017b. Interparticle force analysis on the packing of fine ellipsoids. Powder Technol. 320, 610–624.

Gong, J., Wang, X., Li, L., Nie, Z., 2019. DEM study of the effect of fines content on the small-strain stiffness of gap-graded soils. Comput. Geotech. 112, 35–40.

Gostick, J., Aghighi, M., Hinebaugh, J., Tranter, T., Hoeh, M.A., Day, H., Spellacy, B., Sharqawy, M.H., Bazylak, A., Burns, A., 2016. OpenPNM: a pore network modeling package. Comput. Sci. Eng. 18 (4), 60–74.

Gravish, N., Franklin, S.V., Hu, D.L., Goldman, D.I., 2012. Entangled granular media. Phys. Rev. Lett. 108 (20), 208001.

Hidalgo, R.C., Zuriguel, I., Maza, D., Pagonabarraga, I., 2009. Role of particle shape on the stress propagation in granular packings. Phys. Rev. Lett. 103 (11), 118001.

Imseeh, W.H., Alshibli, K.A., 2018. 3D finite element modelling of force transmission and particle fracture of sand. Comput. Geotech. 94, 184–195.

Kerckhofs, G., Pyka, G., Moesen, M., Schrooten, J., Wevers, M., 2012. High-resolution micro-CT as a tool for 3D surface roughness measurement of 3D additive manufactured porous structures. In: iCT Conf.), pp. 77–83.

Kovalev, O., Gusarov, A., 2017. Modeling of granular packed beds, their statistical analyses and evaluation of effective thermal conductivity. International Journal of Thermal Sciences 114, 327–341.

Lee, C., Suh, H.S., Yoon, B., Yun, T.S., 2017. Particle shape effect on thermal conductivity and shear wave velocity in sands. Acta Geotech. 12 (3), 615–625.

Legland, D., Arganda-Carreras, I., Andrey, P., 2016. MorphoLibJ: integrated library and plugins for mathematical morphology with ImageJ. Bioinformatics 32 (22), 3532–3534.

Lepidi, M., Bacigalupo, A., 2018. Multi-parametric sensitivity analysis of the band structure for tetrachiral acoustic metamaterials. Int. J. Solids Struct. 136–137, 186–202.

Lin, Z., Xu, Z., Liu, P., Liang, Z., Lin, Y.-S., 2020. Polarization-sensitive terahertz resonator using asymmetrical F-shaped metamaterial. Opt. Laser Technol. 121, 105826.

Mirmohammadi, S.A., Behi, M., Gan, Y., Shen, L., 2019. Particle-shape-, temperature-, and concentration-dependent thermal conductivity and viscosity of nanofluids. Phys. Rev. E 99 (4), 043109.

Murphy, K.A., Reiser, N., Choksy, D., Singer, C.E., Jaeger, H.M., 2016. Freestanding loadbearing structures with Z-shaped particles. Granular Matter 18 (2), 26.

Nadimi, S., Fonseca, J., Andò, E., Viggiani, G., 2019. A micro finite-element model for soil behaviour: experimental evaluation for sand under triaxial compression. Géotechnique 1–6.

Newman, M.E., 2003. The structure and function of complex networks. SIAM Rev. 45 (2), 167–256.

Nie, Z., Fang, C., Gong, J., Yin, Z.-Y., 2020. Exploring the effect of particle shape caused by erosion on the shear behaviour of granular materials via the DEM. Int. J. Solids Struct. 202, 1–11.

Otsu, N., 1979. A threshold selection method from gray-level histograms. IEEE Trans. Syst. Man Cybern. 9 (1), 62–66.

Papadopoulos, L., Porter, M.A., Daniels, K.E., Bassett, D.S., 2018. Network analysis of particles and grains. J. Complex Networks 6 (4), 485–565.

Quezada, J.C., Breul, P., Saussine, G., Radjai, F., 2014. Penetration test in coarse granular material using Contact Dynamics Method. Comput. Geotech. 55, 248–253.

Rivier, N., 2006. Extended constraints, arches and soft modes in granular materials. J. Non-Cryst. Solids 352 (42–49), 4505–4508.

Santamarina, J., Cho, G.-C., 2004. Soil behaviour: The role of particle shape. In: Advances in geotechnical engineering: The skempton conference.), vol. 1. Citeseer, pp. 604–617.

Santamarina, J.C., Cho, G.C. Soil behaviour: The role of particle shape. In: Advances in geotechnical engineering: The Skempton conference.), pp. 604–617.

Schreck, C.F., Xu, N., O'hern, C.S., 2010. A comparison of jamming behavior in systems composed of dimer-and ellipse-shaped particles. Soft Matter 6 (13), 2960–2969.

Siu, W., Lee, S.-K., 2000. Effective conductivity computation of a packed bed using constriction resistance and contact angle effects. Int. J. Heat Mass Transf. 43 (21), 3917–3924.

Sundberg, J., Back, P.-E., Ericsson, L.O., Wrafter, J., 2009. Estimation of thermal conductivity and its spatial variability in igneous rocks from in situ density logging. Int. J. Rock Mech. Min. Sci. 46 (6), 1023–1028.

Thorpe, M.F., Duxbury, P.M., 1999. Rigidity theory and applications. Springer Science & Business Media.

Tordesillas, A., Tobin, S.T., Cil, M., Alshibli, K., Behringer, R.P., 2015a. Network flow model of force transmission in unbonded and bonded granular media. Phys. Rev. E 91 (6), 062204.

Tordesillas, A., Tobin, S.T., Cil, M., Alshibli, K., Behringer, R.P., 2015b. Network flow model of force transmission in unbonded and bonded granular media. Phys. Rev. E 91 (6), 062204.

Trepanier, M., Franklin, S.V., 2010. Column collapse of granular rods. Phys. Rev. E 82 (1), 011308.

Van Der Linden, J.H., Narsilio, G.A., Tordesillas, A., 2016. Machine learning framework for analysis of transport through complex networks in porous, granular media: a focus on permeability. Phys. Rev. E 94 (2), 022904.

Vangelatos, Z., Komvopoulos, K., Spanos, J., Farsari, M., Grigoropoulos, C., 2020. Anisotropic and curved lattice members enhance the structural integrity and mechanical performance of architected metamaterials. Int. J. Solids Struct. 193–194, 287–301.

Walker, D.M., Tordesillas, A., 2010. Topological evolution in dense granular materials: a complex networks perspective. Int. J. Solids Struct. 47 (5), 624–639.

Wang, Y., Gao, J., Luo, Z., Brown, T., Zhang, N., 2017. Level-set topology optimization for multimaterial and multifunctional mechanical metamaterials. Eng. Optim. 49 (1), 22–42.

Wiebicke, M., Andò, E., Herle, I., Viggiani, G., 2017. On the metrology of interparticle contacts in sand from x-ray tomography images. Meas. Sci. Technol. 28 (12), 124007.

Young, H.D., Freedman, R.A., Sandin, T., Ford, A.L., 1996. University physics. Addison-Wesley Reading, MA.

Yun, T.S., Evans, T.M., 2010. Three-dimensional random network model for thermal conductivity in particulate materials. Comput. Geotech. 37 (7), 991–998.

Yun, T.S., Santamarina, J.C., 2008. Fundamental study of thermal conduction in dry soils. Granular Matter 10 (3), 197.

Zhang, N., Yu, X., Pradhan, A., Puppala, A.J., 2015. Thermal conductivity of quartz sands by thermo-time domain reflectometry probe and model prediction. J. Mater. Civ. Eng. 27 (12), 04015059.

Zhao, S., Zhang, N., Zhou, X., Zhang, L., 2017. Particle shape effects on fabric of granular random packing. Powder Technol. 310, 175–186.

Zheng, J., Hryciw, R.D., 2016. Segmentation of contacting soil particles in images by modified watershed analysis. Comput. Geotech. 73, 142–152.